Neuron, Volume *57*

Supplemental Data

Embodied Information Processing:

Vibrissa Mechanics and Texture Features

Shape Micro-Motions in Actively Sensing Rats

Jason T. Ritt, Mark L. Andermann, and Christopher I. Moore

Supplemental Experimental Procedures

Here we provide further details of experimental procedures briefly summarized in **Experimental Procedures**.

Videography: Hardware

Cameras

We used two high-speed digital cameras, a MotionScope PCI 8000s (Redlake) 8 bit CCD camera for *ex vivo* measurements, and a pco.1200hs (Cooke Corporation) 10 bit CMOS camera for *in vivo* measurements. Both cameras acquired to ring buffers in onboard RAM (for the acquisition parameters we used, the ring buffer real-time durations were ~8 and 6 seconds for the MotionScope and 1200hs, respectively). After an event of interest, acquisition was halted, the relevant frames were determined by manual playback from the buffers, and the frames written to hard drive for offline analysis (see below for acquisition parameters). Write-to-disk time for a single movie took several minutes. The MotionScope was controlled via Midas acquisition software (Xcitex) that exported data as uncompressed AVI files. The 1200hs was controlled by CamWare (Cooke Corporation), and data exported as a sequence of uncompressed TIFFs.

Lighting

A white incandescent illuminator fed through a bifurcating fiber optic guide and focusing lenses (Dolan Jenner) provided lighting for *ex vivo* recording. We used a pseudo-dark-field technique, placing the lenses above and below the field of view, pointed towards the camera, with the vibrissae between the illuminator and camera. The frames thus acquired were almost entirely black, with the vibrissae appearing as a bright curve, providing a high contrast image for computer tracking.

Lighting during active sensing was provided by a Strobe LED (AOS), a 9x9 grid of pulsed high-power infrared (~880 nm peak wavelength) LEDs. Typical pulse parameters were 20 kHz with a duration of 50 μs, leading to near continuous illumination. Illumination pulses were not synchronized to the camera acquisition. The illuminator was directed upward at a sheet of mylar suspended ~12 cm above. The mylar was in turn positioned ~12 cm below the platform on which the rat was placed. In this arrangement, the rat head and vibrissae were dark against a bright background, facilitating computer tracking.

Simulated Rat: *Ex Vivo* Videography

To achieve precise control over vibrissae motions for studies of basic features of micro-motions, plucked vibrissae were taken from rats terminated in the course of other experiments, (Sprague Dawley, 300-500g) and driven over surfaces with a precision motor with custom integrated gearbox (Maxon: Figure 1A). A variable DC power supply (Tenma 72-6628) controlled the motor. A small stick attached perpendicular to the motor shaft traveled through an IR

emitter/phototransistor pair (DigiKey QVE11233). We monitored the amplified output of the phototransistor through an oscilloscope (LeCroy LA302) and adjusted the power supply to achieve the desired frequency of motion. Recordings were conducted when the frequency was stably within 0.2 Hz of the target frequency. For analysis, these frequencies were converted to angular sweep speeds. We verified precision of motor rotation in separate recordings of a marked point on the motor shaft (not shown).

Based on initial pilot sessions, we set MotionScope acquisition to 4000 frames/sec, at either 98x100 or 68x160 pixel resolution, for all reported *ex vivo* data. Most videos were acquired with a 50mm/f1.2 lens at ~30cm distance resulting in 0.321 mm per pixel resolution (e.g. Figure 1A right), as measured via separate videos with a ruler in the plane of focus. A subset of high-magnification videos used a 135mm lens at ~2 meters distance resulting in 0.056 mm per pixel resolution (e.g. Figure 5A).

Behaving Rat: Videography During Active Sensation

Using the *ex vivo* data as guide, we conducted pilot sessions with four naïve animals that explored (out of novelty) a textured surface (not shown). Using videography acquisition parameters based on these animals, we then began training the texture task, as described in Methods in the main text. Some additional details are provided here. Textures were cleaned prior to every session (with careful application of 70% isopropanol, then blown dry with compressed air), and in some cases replaced with a new discriminandum milled with the same exact textures as previous training (i.e. with the same realization of the random depth profile). Lick detection was provided by custom hardware that indicated when the rat's hind paws and tongue completed a low-voltage circuit between a stainless steel plate on the platform and one of the stainless steel tips of the reward tubes. Reward was provided by two independently controlled 60mL syringes in high velocity syringe pumps (Med Associates) fed through ~40cm of small diameter tubing to the reward tips; pumps were routinely calibrated, with typical delivery for a single reward ~80 to 100μL.

Data Analysis

The very high frame rates used in this study, necessary to capture fast mechanical events in the vibrissae, precluded manual vibrissa tracking and analysis. We therefore devoted significant effort to developing tracking software (in Matlab). Nyquist frequency requirements suggest 1000 frames per second should be sufficient to capture motions up to 500Hz, as reported here. However, this result holds only asymptotically, and we found in practice that substantially higher frame rates were needed to obtain sufficient signal to noise for the fast transient motions we observed both *ex vivo* and *in vivo*. Moreover, we found occasional single ringing epochs up to 1kHz, highlighting the importance of high temporal resolution for accurate assessment of vibrissa micro-motions. All videos were intensity normalized by background frames (without vibrissa or rat in view) before subsequent analysis.

For *ex vivo* movies, we manually determined the motor center, formed circles of various radii around this center, and measured the vibrissa at its intersection with a given radius (a bright point on the circle). In each frame, the angle of the vibrissa was determined from the center of mass of intensities in a small neighborhood around the peak intensity on the circle. This generated angle measurements as a function of time, including both the sweeping motion and micro-motions. We subtracted the sweep speed related angular displacement to form "residual angles", as plotted in Figure 1D (e.g. θ Residual(t) = θ Measured(t) - 720*t for a sweep speed of 720^{o}/sec).

For *in vivo* movies, we developed a more advanced analysis, as the vibrissae are translated due to head motion in addition to rotations due to whisking. Within a given initial frame, a seed was manually selected for the vibrissa base, as was a second point along the vibrissa. The tracker then iteratively worked outward along the vibrissa, laying successive 4 pixel (~0.44mm) length

segments, as follows. At each iteration, the distal end of the last defined segment served as a common endpoint of a collection of new segments in a range of angles around the last segment angle (relative to the video frame). The new segment with the lowest average intensity was taken as the next vibrissa segment, and the process repeated. Intensities at non-integral locations in the frame were determined by bicubic interpolation of the neighboring four pixels. Importantly, the endpoints of the segments were not quantized to pixel locations, and the effective averaging over a region of pixels provided sub-pixel resolution. The tracker continued in each frame until going below a manually set intensity threshold, defining the end of the track-able portion of the vibrissa. Occasionally tracking continued well past the vibrissa tip (an example occurs in Supplemental Movie S2), but since iteration occurred outward from the face this did not affect analysis, e.g. at 5mm from the base. In the next frame, the tracker sampled perpendicular to the line established by the first two segments (proximal to the base) from the previous frame to find the new base segment. The base of the vibrissa in the new frame was found by applying an edge detection algorithm to locate the border of the face. With the new base defined, tracking resumed outward along the vibrissa.

After tracking was completed, the end of the track in a given frame was clipped at the intersection of the vibrissa with the sensory surface, removing all line segments past this juncture. In most cases, tracker noise due to fluctuations in pixel intensities was reduced by averaging neighboring segments. All tracks were manually verified by playing back the video with the tracked vibrissa overlaid. In a handful of frames across all analyzed movies, the track would be radically misplaced due to random fluctuation in the images. On those frames, the track was set to the average of positions in the preceding and following frames. We took human confirmation of tracking quality as our gold standard, since there is no unique mathematical solution.

This approach was robust to transverse intersections with other vibrissae along the length of the vibrissa (see Supplemental Movie S2; note that for display purposes tracked points are quantized to pixel locations and represented by multi-pixel crosses, but all analyses used sub-pixel tracks), but was not robust to tangential intersections or overlaps near the base, a specifically challenging aspect of vibrissa tracking (see also (Knutsen et al., 2006)). As such, this method worked best for shorter and more anterior vibrissae, where overlap at the base was less common. The principal virtue of this method was that it could capture arbitrary changes in the vibrissa shape with high precision.

Ahissar and colleagues (Knutsen et al., 2005) developed a sophisticated system for vibrissa tracking that is suited to larger amplitude vibrissa motion and relatively slower events such as whisking and sustained contact bending. This approach was not appropriate for the current study for several reasons. Their tracker employs a low dimensional spline representation, which would smooth over the micro-motions we analyze here (and would prohibit further analyses such as visualization of traveling impulses). Moreover, to achieve reasonable computation times, the precision of this tracker was limited to a subset of pixel values (i.e., quantized). Because visualization of low-amplitude, high-velocity events riding on larger, lower frequency vibrissa motions induced a trade-off of image size with frame rate that required sub-pixel resolution (obtained by suitable averaging of intensities in a neighborhood of the tracked point, as described above), we developed an approach more suited to our needs. We note that we also tried several spline-based tracking methods before utilizing the method presented here, including a frame by frame non-linear optimization similar to (Knutsen et al., 2005), and a Bayesian particle filter that either introduced high tracking jitter or smoothed unacceptably over transient motions depending on parameter settings.

Relative to other vibrissa monitoring techniques such as linear CCD arrays with head fixed animals (Harvey et al., 2001), videography is a low yield technique. The principal bottleneck is the time it takes to save frames from camera memory to permanent hard-drive storage, which limits us to a small number of trials. However, substantial benefits include the ability to make

careful comparisons of head and vibrissa positions to analyze data in head centered coordinates. CCD techniques require the head to be in a known position, either by head fixing the animal or training it to do a stereotyped nose poked at the time of data acquisition. Through videography we allow the animal free range of interaction with the surface. Moreover, videography provides measurement along the entire length of the vibrissa, for example to see differences in point of contact vs. face angle motions (see Figure 3).

To measure velocities, rise times and amplitudes of micro-motions during surface contact (Figures 7 and 8), we took tracked vibrissae and estimated the angle of the face at the vibrissa base by calculating the gradient of intensity in a small window around the vibrissa base point (after blurring with a narrow Gaussian to suppress noise). By subtracting the position of the vibrissa base and rotating the frame by the angle of the face, we put each vibrissa in head centered coordinates. In the absence of whisking or micro-motions, replay of this aligned movie shows a stationary vibrissa across time. We then converted the tracked position at each segment to an angle in this coordinate frame, typically emphasizing measurement 5 mm from the base for comparison with anesthetized studies where deflections are often initiated at this position (Andermann and Moore, 2006; Pinto et al., 2000).

To separate whisks from micro-motions in this head-centered timeseries, we used a generalized additive model (Hastie et al., 2001), in which the vibrissa motion was assumed to be the sum of two spline components, that minimized a weighted combination of the error (sum of squared residuals) and the average second derivative of the splines (smoothness). One spline was weighted towards greater smoothness (lower frequency), corresponding to whisking motions, and the other was weighted towards lower error (higher frequency), capturing micro-motions. Weight values were chosen manually after search using a generalized cross validation procedure that balanced the bias against the variance of the fit. In this procedure, the fits were repeatedly computed while excluding different points from the original timeseries, and the squared errors at those points summed. In practice, the chosen weights corresponded to a break between whisking and micro-motion components at ~50 Hz. The model was fit using a backfitting algorithm (Hastie et al., 2001) that simultaneously estimated both spline components. All analysis was performed on the micro-motion component, in which "zero" meant no motion beyond the slower 'whisking' sweep speed. In practice we found a small leakage from the whisking component into the micro-motion component, so that "rest" was defined as the average of upper and lower envelopes of the micro-motion component, in a procedure akin to empirical mode decomposition (Huang et al., 1998). This analysis was robust to changes in set point, and detected only the fast micro-motions that were putatively due to surface interaction. We then found all crossings through rest (linearly interpolated between successive time points of opposite sign, rejecting crossings with fewer than three timepoints), and fit, via least-squares, a 2^{nd} order polynomial between each pair of crossings. The second order fits captured the successive micro-motions well (see Figure 7) while providing an estimate of derivatives more robust to noise than simple discrete differencing of the timeseries. Micro-motion amplitudes and rise times were then defined as, respectively, the maximum absolute displacement of the fit and the time from rest crossing to maximum displacement. The velocities were defined as the absolute slope of the fit at onset (the peak velocity of each micro-motion); for a symmetric 2^{nd} order fit, this is twice the average velocity. To compare stimulus parameters in previous studies (Figure 8B *right*), we took the reported peak velocities and onset durations. Rise time was defined as the time from rest to reach maximal excursion. For a ramp-and-hold, the peak velocity is the slope of the ON ramp (or reported peak velocity when analyzed separately due to stimulator filtering), and the rise time is the time to reach plateau. For a sinusoid centered at the vibrissa resting position, the peak velocity occurs at the zero crossing, and the rise times is a quarter cycle of the sine wave. For a sinusoid offset to begin with a trough (as in (Stuttgen et al., 2006)), the peak velocity occurs at half the time of rise, and the rise time is a half-cycle.

For *in vivo* frequency estimates (Figures 4, 5 and 6), we increased the number of vibrissae that could be measured in a given trial by setting a horizontal line immediately adjacent (~1 mm) and parallel to the surface. We then tracked vibrissa intersections with this line, similar to the radius technique applied to *ex vivo* movies. In this way, we were not hampered by overlap in vibrissa images near the base. This produced a timeseries of vibrissa position along the line, which we high pass filtered at 50 Hz to remove whisking and head translations, and low passed at 800 Hz to reduce high frequency noise. We then used a Hilbert transform (Cohen, 1995) of the timeseries to find instantaneous frequencies and amplitudes at each time point. We found the average frequency for the timeseries by taking the average of the instantaneous frequencies weighted by the instantaneous squared amplitudes. The amplitude squared is a measure of oscillation power, similar to the power spectral density in Fourier analysis. This method appropriately estimates frequencies of intermittent micro-motion epochs such as we observed, and rejected small amplitude high frequency noise from the estimate.

We estimated lengths by selecting one or more frames with the vibrissa not in surface contact, and used a custom GUI (in Matlab) to select ~10-15 points along the shaft. The distances between these points were summed to provide an estimate of vibrissa length. The procedure was repeated three times for each vibrissae. The CV (standard deviation divided by mean over the three estimates) was typically below 1%, indicating that manual selection of points was not a significant source of error. Another source of error is that the vibrissae do not lie exactly in the plane of focus, and hence we are actually measuring their projection. One limit to the magnitude of this error is that the short exposure times we used required an open aperture, reducing our depth of field such that most observable (in focus) vibrissa remained close to the imaged plane. From comparison of videographical estimated lengths with true lengths measured directly on a euthenized animal, we found video-determined lengths to be slightly underestimated, with an error on the order of 10% (not shown).

To avoid any possible corruption of the intrinsic vibrissa properties that are a focus of this study, we did not paint or otherwise alter vibrissa for videographic identification. Arc identity was usually accessible from manual viewing of the video, but as we were not as confident of arc identity, and because length (more robustly estimated from the video) is a stronger determinant of elastic properties, most analyses (beyond contact probabilities) are in terms of length only. However, we refined our ability to properly identify vibrissa by taking video of a euthenized animal with the same video parameters as used during behavior sessions, and comparing the videographic reconstruction to individual videos in which we touched each vibrissa in turn (using the true identity from direct examination of the face). Building on this process, in a subset of videos corresponding to a single session with rat 4B, we estimated contact probabilities by vibrissa identity (Figure 2) through extensive manual analysis. A keyframe was selected with the complete pad on at least one side of the face in view, and the individual vibrissae identified from position, depth-from-focus, and structure from motion cues. With this keyframe as a guide to identity, we determined whether or not each vibrissa contacted the surface during the animal's approach. We defined Contact as being able to see the tip and detecting at least minimal bending of the shaft with the tip near the surface. We defined No Contact as seeing the tip clearly away from the surface (or out of the frame entirely, with the shaft clearly orientated away from the surface). If neither of these conditions held we labeled the contact as Undetermined; because of this category, contact probabilities do not add up to 1. More anterior (5 arc and above) and ventral vibrissae (E row) were not quantified in this analysis because they were not reliably imaged.

Figure S1. Example Plots of Behavioral Performance

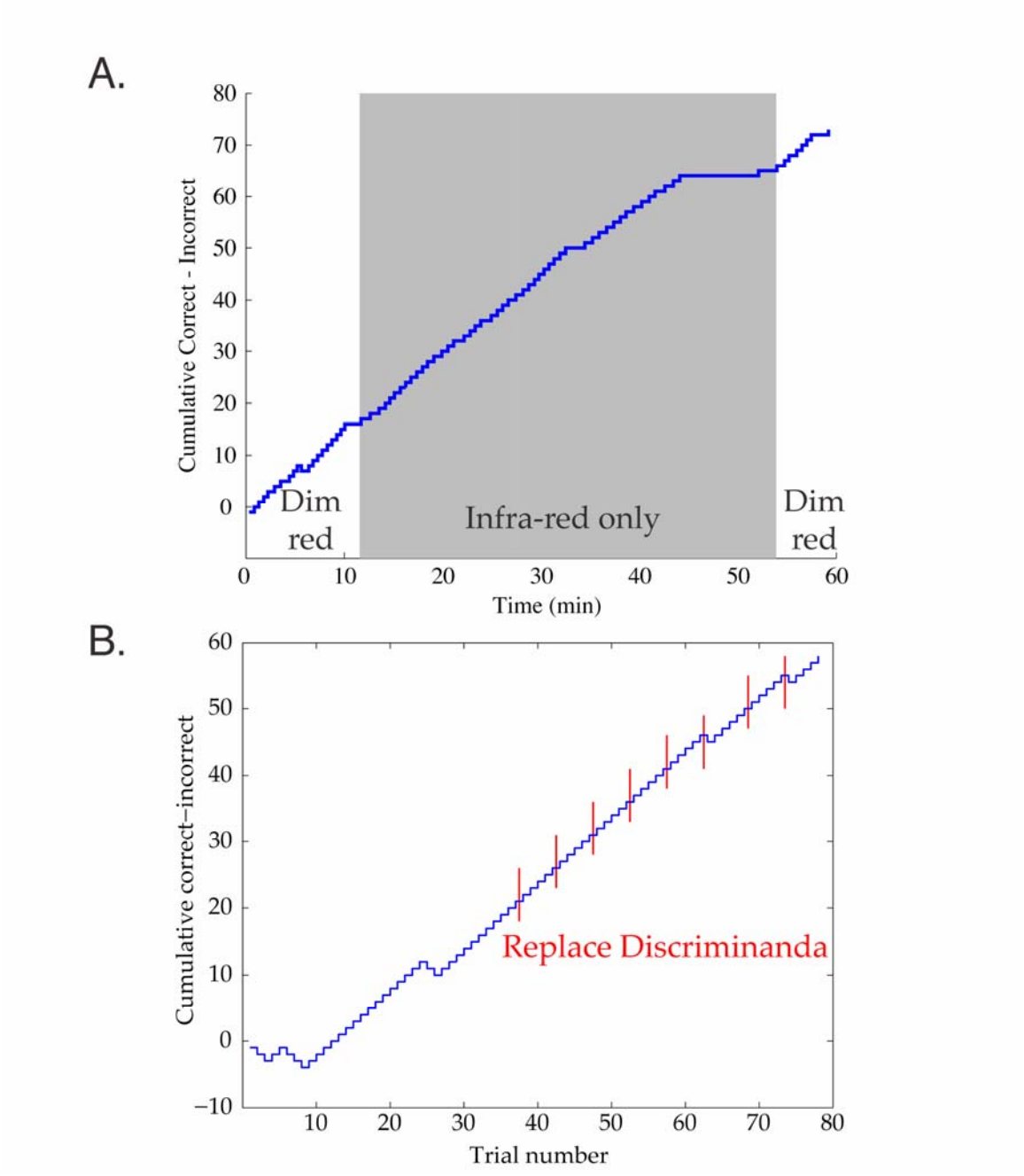

(A) The cumulative number of correct trials minus incorrect trials as a function of time, over a session for one rat, shows the high performance capabilities of trained animals. The graph increments by one with each correct response and decrements by one for each incorrect response, with only one incorrect response (around minute 6) out of ~70 trials over 60 minutes in this session. In the shaded area, the dim red illumination normally used in the session was turned off and the operator used night vision goggles under infra-red illumination only (the difficulty of working under night vision goggles, for example from eye strain, precluded universal use of infra-red in all sessions). Performance was unchanged, indicating that vision is not required for task performance (similar results were obtained with all three rats). During the plateau around minute 45, the rat engaged in non-task behaviors (e.g. grooming, undirected exploration) before resuming task participation around minute 52.
(B) In a session for a different rat trained to discriminate smooth surfaces from 4mm gratings, new discriminanda (new objects with the same textures as in its previous training) were swapped in at the times indicated by the vertical red lines, without cue. Performance is shown versus trial number instead of time for clarity. A rat using non-textural information, such as object odor, would show a decrease in performance during the swaps, but instead performance remained well above criterion (performance over entire session: 87% (68/78); in trials before beginning swaps: 78% (29/37); in trials after beginning swaps 95% (39/41)). The apparent increase in performance results from several incorrect trials at the very beginning of the session, when the rat was highly exploratory and not yet fully engaged in the task; the important point is that performance does not decrease with swapped discriminanda.

Supplemental References

Andermann, M. L., and Moore, C. I. (2006). A somatotopic map of vibrissa motion direction within a barrel column. Nat Neurosci *9*, 543-551.

Cohen, L. (1995). Time-frequency analysis (Engelwood Cliffs, N.J., Prentice-Hall).

Harvey, M. A., Bermejo, R., and Zeigler, H. P. (2001). Discriminative whisking in the head-fixed rat: optoelectronic monitoring during tactile detection and discrimination tasks. Somatosens Mot Res *18*, 211-222.

Hastie, T., Tibshirani, R., and Friedman, J. (2001). The Elements of Statistical Learning (New York, Springer-Verlag).

Huang, N. E., Shen, Z., Long, S. R., Wu, M. C., Shih, H. H., Zheng, Q., Yen, N.-C., Tung, C. C., and Liu, H. H. (1998). The empirical mode decomposition and the Hilbert spectrum for nonlinear and non-stationary time series analysis. Proc Roy Soc A *454*, 903-995.

Knutsen, P. M., Derdikman, D., and Ahissar, E. (2005). Tracking whisker and head movements in unrestrained behaving rodents. J Neurophysiol *93*, 2294-2301.

Knutsen, P. M., Pietr, M., and Ahissar, E. (2006). Haptic object localization in the vibrissal system: behavior and performance. J Neurosci *26*, 8451-8464.

Pinto, D. J., Brumberg, J. C., and Simons, D. J. (2000). Circuit dynamics and coding strategies in rodent somatosensory cortex. J Neurophysiol *83*, 1158-1166.

Stuttgen, M. C., Ruter, J., and Schwarz, C. (2006). Two psychophysical channels of whisker deflection align with two neuronal classes of primary afferents. Journal of Neuroscience *26*, 7933-7941.